doi:10.1093/brain/aws281 Brain 2012: 135; 3699–3711 | 3699

BRAIN
A JOURNAL OF NEUROLOGY

Resting state functional connectivity of the striatum in Parkinson's disease

Carl D. Hacker,[1] Joel S. Perlmutter,[2,3] Susan R. Criswell,[3] Beau M. Ances[3] and Abraham Z. Snyder[2,3]

1 Department of Biomedical Engineering, Washington University School of Medicine, Saint Louis, MO 63110, USA
2 Department of Radiology, Washington University School of Medicine, Saint Louis, MO 63110, USA
3 Department of Neurology, Washington University School of Medicine, Saint Louis, MO 63110, USA

Correspondence to: Abraham Snyder, Ph.D. M.D.
Department of Radiology,
Washington University School of Medicine,
Campus Box 8225,
4535 Scott Avenue,
Saint Louis,
MO 63110, USA
E-mail: avi@npg.wustl.edu

Classical accounts of the pathophysiology of Parkinson's disease have emphasized degeneration of dopaminergic nigrostriatal neurons with consequent dysfunction of cortico–striatal–thalamic loops. In contrast, post-mortem studies indicate that pathological changes in Parkinson's disease (Lewy neurites and Lewy bodies) first appear primarily in the lower brainstem with subsequent progression to more rostral parts of the neuraxis. The nigrostriatal and histological perspectives are not incompatible, but they do emphasize different anatomical structures. To address the question of which brain structures are functionally most affected by Parkinson's disease, we performed a resting-state functional magnetic resonance imaging study focused on striatal functional connectivity. We contrasted 13 patients with advanced Parkinson's disease versus 19 age-matched control subjects, using methodology incorporating scrupulous attention to minimizing the effects of head motion during scanning. The principal finding in the Parkinson's disease group was markedly lower striatal correlations with thalamus, midbrain, pons and cerebellum. This result reinforces the importance of the brainstem in the pathophysiology of Parkinson's disease. Focally altered functional connectivity also was observed in sensori-motor and visual areas of the cerebral cortex, as well the supramarginal gyrus. Striatal functional connectivity with the brainstem was graded (posterior putamen > anterior putamen > caudate), in both patients with Parkinson's disease and control subjects, in a manner that corresponds to well-documented gradient of striatal dopaminergic function loss in Parkinson's disease. We hypothesize that this gradient provides a clue to the pathogenesis of Parkinson's disease.

Keywords: Parkinson's disease; functional MRI; striatum; brainstem; functional reorganization
Abbreviation: UPDRS = Unified Parkinson's Disease Rating Scale

Introduction

Parkinson's disease is a progressive neurodegenerative disorder manifesting principally as resting tremor, rigidity, akinesia and postural instability (Jankovic, 2008). Classical accounts of the pathophysiology of Parkinson's disease have emphasized degeneration of dopaminergic nigrostriatal neurons (Damier *et al*., 1999) with consequent dysfunction of cortico–striatal–thalamic loops (Alexander *et al*., 1986; Albin *et al*., 1989; Berardelli *et al*., 2001; Mink, 2003; Jankovic, 2008). Post-mortem studies indicate

Received February 28, 2012. Revised July 25, 2012. Accepted August 23, 2012

that pathological changes in Parkinson's disease (Lewy neurites and Lewy bodies) first appear primarily in the lower brainstem with subsequent progression to more rostral parts of the neuraxis (Braak *et al*., 2004). Motor manifestations of Parkinson's disease become apparent only after the disease process reaches the midbrain with degeneration of nigrostriatal neurons (Del Tredici *et al*., 2002). Parkinson's disease also includes multiple non-motor manifestations that reflect dysfunction beyond the nigrostriatal pathway. The nigrostriatal and histological perspectives are not incompatible, but they do emphasize different anatomical structures.

Neuroimaging of Parkinson's disease historically has been dominated by positron emission tomography (PET) and single-photon emission computed tomography (SPECT) studies using a variety of dopaminergic radiopharmaceuticals that focus on striatal measures of nigrostriatal neurons (Nandhagopal *et al*., 2008). Concurrently, fluorodeoxyglucose-PET has been used to image abnormal covariance patterns of cortical and subcortical regional metabolism that correlate with motor and cognitive impairment (Eidelberg, 2009). Conventional (T_1- and T_2-weighted) MRI has provided only limited information (Stoessl, 2011), although abnormalities in the substantia nigra have recently been shown using diffusion tensor MRI (Brooks and Pavese, 2011; Rolheiser *et al*., 2011). Functional MRI of Parkinson's disease is a relatively recent development (Stoessl, 2009). Enhanced responses to finger-sequencing tasks in participants with Parkinson's disease, compared with control subjects, have been reported in primary and supplementary motor areas (Catalan *et al*., 1999; Turner *et al*., 2003; Wu and Hallett, 2005; Lewis *et al*., 2011) and basal ganglia (Turner *et al*., 2003; Lewis *et al*., 2011). However, precision grip tasks elicit decreased responses in these same areas (Yu *et al*., 2007; Prodoehl *et al*., 2010). Such variable group contrast effects present interpretive difficulties. Perhaps more critically, a 'chicken versus egg' ambiguity confounds all task-based neuroimaging studies of functional deficits. Does a change in regional brain function associated with an abnormally performed task reflect dysfunction of that brain region, or does it reflect the altered performance of the task? For example, motor tasks elicit reduced responses in supplementary motor area in akinetic patients with Parkinson's disease (Grafton, 2004), but does this reflect impaired task performance, or do the reduced responses directly reflect supplementary motor area dysfunction?

Resting-state functional connectivity functional MRI offers a means of assessing the status of functional systems within the brain without the interpretive confound of variable task performance (Fox and Greicius, 2010; Zhang and Raichle, 2010). In application to Alzheimer's disease, numerous resting-state functional connectivity functional MRI studies have demonstrated reduced functional connectivity primarily within the default mode network (for review see Mevel *et al*., 2011). This result is concordant with the known distribution of Alzheimer's disease histopathology (Buckner *et al*., 2005; Nelson *et al*., 2009; Shin *et al*., 2011). Moreover, default mode network functionality is central to episodic memory (Buckner *et al*., 2008), which is precisely the cognitive domain that characteristically is impaired in Alzheimer's disease. Thus, in Alzheimer's disease, the locus of greatest pathology, the characteristic cognitive deficit and the topography of the most prominent resting-state functional connectivity functional MRI abnormalities all coincide.

The current understanding of Parkinson's disease is much less coherent. The brainstem is the locus of greatest pathology, but cortico–striatal–thalamic loop dysfunction is most often invoked to explain clinical deficits. Resting-state functional MRI could potentially inform this question. To date, only a handful of articles (Wu *et al*., 2009; Helmich *et al*., 2010; Kwak *et al*., 2010; Skidmore *et al*., 2011) compare Parkinson's disease with age-matched control subjects, most of which report relatively reduced functional connectivity in Parkinson's disease, either globally (Skidmore *et al*., 2011) or within specific cortical resting-state networks (van Eimeren *et al*., 2009). None of these studies specifically address the brainstem or illuminate the question of how the distribution of histopathology affects resting-state networks. Here, we map striatal functional connectivity in a group of participants with Parkinson's disease with advanced disease and a comparison group of age-matched control subjects. We ask whether the manifestations of Parkinson's disease, as assessed by resting-state functional connectivity MRI, implicate predominantly cortico–striatal–thalamic circuits or, alternatively, more caudal structures.

Materials and methods

Participants

Patients with Parkinson's disease were recruited from the Movement Disorders Centre at Washington University School of Medicine. All had a diagnosis of idiopathic Parkinson's disease according to standard clinical criteria (Hughes *et al*., 1992). To minimize the impact of head motion, patients with Parkinson's disease were studied while taking their usual medications. A total of 31 Parkinson's disease functional MRI data sets were acquired, but 18 were excluded from the present analyses because they did not meet stringent quality assurance criteria (see later in text). The present results include 13 subjects with Parkinson's disease (nine male, age: 63.4 ± 9.3 years) with advanced disease [mean Unified Parkinson's Disease Rating Scale (UPDRS) III score = 39.1 OFF medication, 20.7 ON medication, maximum possible = 108] studied before implantation of deep brain stimulation electrodes. All patients were unambiguously responsive to L-3,4-dihydroxyphenylalanine (L-DOPA) and not tremor dominant (mean UPDRS tremor score = 4.2 OFF medication, 1.7 ON medication, maximum possible = 28). A total of 24 control data sets were acquired (five excluded and 19 included, 12 male, age = 65.8 ± 9.7 years). Control participants were recruited from the Movement Disorders Centre and the Knight Alzheimer's Disease Research Centre at Washington University. Control participants did not have parkinsonism as determined by neurological exam (UPDRS III score <3 and no postural or action tremor). Control participant data were selected for inclusion in the study with the objective of matching the Parkinson's disease group with respect to age, gender and functional MRI data quality assurance measures (see later in text). Table 1 contains additional demographic details. All participants had normal structural images and were cognitively normal by clinical examination and the modified Mini-Mental State Examination (Teng and Chui, 1987). All participants provided written informed consent in accordance with the Declaration of Helsinki. All aspects of the study were approved by the Washington University School of Medicine Human Studies Institutional Review Board.

Table 1 Study cohort demographics

Measure	Normal control subjects	Subjects with Parkinson's disease
Age (years)	65.8 ± 9.7	63.4 ± 9.3
Gender, male:female	12:7	9:4
Handedness, right:left	18:1	10:3
Age of onset (years)	N/A	50.5 ± 8.3
Affected side, right:left	N/A	6:7
Duration of disease (years)	N/A	12.9
UPDRS III score (ON)	N/A	20.7 ± 7.1
UPDRS III score (OFF)	<3	39.1 ± 9.4
UPDRS III tremor score (ON)	N/A	1.7
UPDRS III tremor score (OFF)	N/A	4.2

N/A = not applicable.

Neuroimaging data acquisition

Magnetic resonance images were acquired with a 3 T Trio scanner (Siemens) equipped with a standard 12-channel head coil. Each participant contributed two or three 6-min resting-state functional MRI runs (164 volumes/run, echo time = 27 ms, repetition time = 2200 ms, field of view = 256 mm, flip angle = 90°, 4-mm cubic voxels) during which they were instructed to fixate on a visual crosshair, remain still and not fall asleep. Anatomical imaging included one sagittal T_1-weighted magnetization-prepared rapid acquisition gradient echo (MP-RAGE) scan (T_1-weighted) (echo time = 16 ms, repetition time = 2400 ms, inversion time = 1000 ms, flip angle = 8°, 1 × 1 × 1-mm voxels) and one T_2-weighted 3D scan (echo time = 455 ms, repetition time = 3200 ms, 1 × 1 × 1-mm voxels).

Preprocessing of resting-state functional magnetic resonance imaging

Initial functional MRI preprocessing followed conventional practice as previously described (Shulman *et al*., 2010). Briefly, this included compensation for slice-dependent time shifts, elimination of systematic odd–even slice intensity differences due to interleaved acquisition and rigid body correction for head movement within and across runs. The functional MRI data were intensity scaled (one multiplicative factor applied to all voxels of all frames within each run) to obtain a mode value of 1000 (Ojemann *et al*., 1997). This scaling enabled assessment of voxel-wise variance for purposes of quality assurance but did not alter computed correlations. Atlas transformation was achieved by composition of affine transforms derived by a sequence of co-registration involving the functional MRI volumes, the T_2-weighted and T_1-weighted structural images and an atlas representative template (Shulman *et al*., 2010). Head movement correction was included in a single resampling that generated volumetric time series in (3 mm^3) atlas space. To minimize group-specific atlas registration bias, the atlas representative template was generated from study-derived MP-RAGE data (patients with Parkinson's disease and controls) as detailed previously (Buckner *et al*., 2004). Currently reported coordinates represent Talairach atlas space as defined by the spatial normalization method of Lancaster *et al*. (1995).

Additional preprocessing in preparation for correlation mapping included spatial smoothing (6-mm full-width at half-maximum Gaussian blur in each direction), voxel-wise removal of linear trends over each functional MRI run and temporal low-pass filtering retaining frequencies <0.1 Hz. Spurious variance was reduced by regression of nuisance waveforms derived from head motion correction and the time series extracted from regions (of 'non-interest') in white matter and CSF. This regression step also included the time series averaged over the whole brain. Thus, all subsequently computed correlations were effectively partial correlations of order 1 controlling for widely shared variance. Whole-brain signal regression offers the advantage of enhancing the spatial specificity of functional connectivity mapping especially in the case of subcortical seed regions (Fox *et al*., 2009). However, a consequence of this technique is that positive and negative values are approximately balanced in computed correlation maps, although the topography of these maps is unconstrained, and differences between groups are unbiased. Additional discussion of whole-brain signal regression is given in the Supplementary material.

Quality assurance

Particular care was taken to minimize the impact of subject head motion at the individual and at the group levels. For each subject with at least two low-motion functional MRI runs, we evaluated root mean square head motion (in mm) as determined by the realignment procedure, as well as the voxel-wise time series standard deviation (SD) averaged over the whole brain (see Supplementary material for methodological details). Quality assurance-based exclusion criteria were empirically determined with the objective of maximizing the number of included subjects while simultaneously excluding subjects with excessive head motion. Subjects with a whole-brain mean functional MRI signal SD > 0.6% (after nuisance regression) or root mean square movement >0.6 mm were excluded. Applying these quality assurance criteria left 13 of 31 patients with Parkinson's disease and 19 of 24 control subjects. The finally obtained quality assurance measure distributions were comparable across the Parkinson's disease and control groups (Supplementary Fig. 1).

Demarcation of striatal seed regions

Striatal seed regions of interest were manually segmented for each subject on T_1- and T_2-weighted images displayed in atlas space (1-mm cubic voxels) using the region of interest tool in Analyze 8.5 (http://mayoresearch.mayo.edu/robb_lab/analyze.cfm). All region of interest segmentations were performed by a single operator blinded to subject identity. Regions of interest were defined bilaterally in (i) caudate nucleus; (ii) anterior putamen; and (iii) posterior putamen. Voxels within 2 mm of the lateral ventricle were excluded. The boundary between anterior and posterior putamen was taken to be the posterior aspect of the fornix in the axial plane (Fig. 1). Regions of interest (six per subject), so demarcated in 1-mm^3 atlas space, were resampled to 3-mm^3 atlas space to enable extraction of time series from each subject's functional MRI data.

Correlation mapping

Correlation maps were computed according to standard practice using time series extracted from seed regions of interest by averaging over all included voxels (Biswal *et al*., 1995; Vincent *et al*., 2006). Here, the procedure was slightly modified to account for the presence of punctate foci of unusually high signal variance (up to 100 times the region of interest mean), most likely representing lenticulo-striate vessels. Voxels in which the signal SD exceeded 0.4% (almost always a minor fraction of each region of interest) were excluded from the

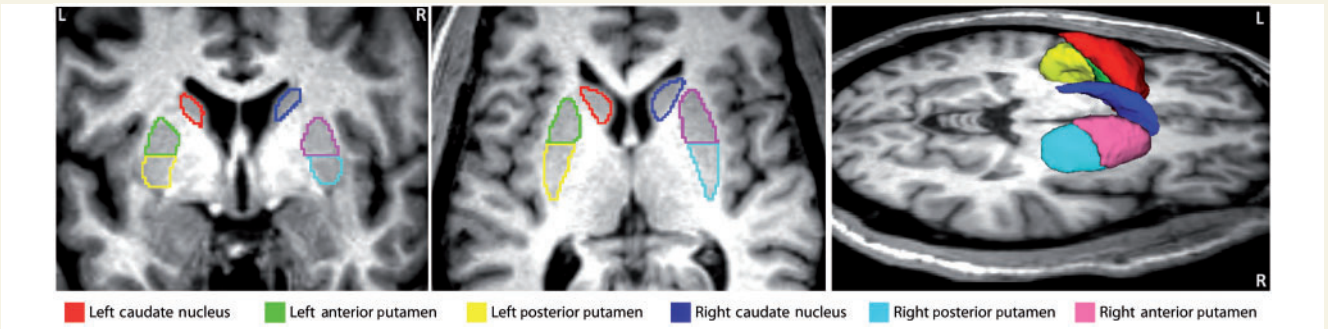

Figure 1 Striatal seed regions of interest defined in a representative control subject. Region of interest boundaries were manually traced on T_1-weighted images using Analyze 8.5 as illustrated in the *left* and *middle* panels. The boundary between anterior and posterior putamen was taken to be the posterior aspect of the fornix. Brain left is shown on the image left. Six regions of interest were defined in each subject: left caudate (red), left anterior putamen (green), left posterior putamen (yellow), right caudate (dark blue), right anterior putamen (pink) and right posterior putamen (light blue). The *right* panel shows a 3D rendering of the same regions of interest generated using 3D Slicer (http://www.slicer.org).

region of interest time series. Correlation maps were conventionally computed using the Pearson product moment formula (Fox *et al.*, 2005). Fisher *z*-transform $\{z(r) = 0.5\ln [(1 + r)/(1 - r)]\}$ was applied before further analyses.

Statistical analysis

For each seed, group mean correlation maps were computed by averaging $z(r)$ maps over subjects. Parkinson's disease versus control differences were examined using group difference $z(r)$ maps. Gaussianized *t*-statistic (*Z*-score) maps (random effects analyses) were used to obtain a more rigorous assessment of group differences. Statistical significance, accounting for comparisons over multiple voxels, was assessed on a cluster-wise basis using extent and *Z*-score thresholds computed by extensive permutation resampling over subjects (see Supplementary material and Supplementary Fig. 2).

Results

Demographic variables

The Parkinson's disease and control groups were well matched in age and sex distributions (Table 1). None of the six regions of interest showed a statistically significant group difference in volume (two-sided *t*-test) after Bonferroni correction. Indices of functional MRI data quality (head movement during scanning and voxel-wise temporal variance) were well matched across the two groups (Supplementary Fig. 1).

Resting-state functional connectivity magnetic resonance imaging in control subjects

Striatal functional connectivity in the control group generally was consistent with previous reports (Di Martino *et al.*, 2008; Kelly *et al.*, 2009; Barnes *et al.*, 2010). All six striatal seed regions yielded bilaterally symmetric correlation maps (Fig. 2) with positive and negative maxima in specific parts of the cerebral cortex plus strictly positive correlations in subcortical structures. Striatal functional connectivity with other brain regions followed established neuroanatomical principles. Thus, the caudate showed strong correlations with anterior cingulate cortex, fronto-polar regions and anterior thalamus. In contrast, the posterior putamen was most strongly correlated with the supramarginal gyrus, posterior thalamus and a contiguous region of grey matter extending from the thalamus, through the midbrain, pons and cerebellum. For descriptive purposes, we define this contiguous region as the 'extended brainstem'. The anterior putamen exhibited a pattern of functional connectivity intermediate between caudate and posterior putamen. All striatal subdivisions were negatively correlated with sensori-motor cortex and cortical visual areas; the putamen was negatively correlated with subgenual prefrontal cortex.

Resting-state functional connectivity magnetic resonance imaging in patients with Parkinson's disease

Striatal functional connectivity in the Parkinson's disease group was markedly altered (Fig. 2). Clusters of contiguous voxels satisfying rigorous statistical criteria for group-level contrasts are shown in Fig. 3. The most prominent group effect was weaker correlations between all striatal seeds and the extended brainstem in the Parkinson's disease group (Figs 2 and 3 and Supplementary Fig. 3 and 4). This effect manifested throughout the extended brainstem, respecting anatomical boundaries (i.e. did not cross the tentorium or enter CSF spaces). In the cerebellum, the group contrast effect followed the dual somatomotor representations in superior and inferior lobules (Ramnani, 2006; Buckner *et al.*, 2011) (Fig. 3, left posterior putamen seed, $x = -33$). To examine this result in greater detail, correlations obtained for striatal seeds in both groups were averaged over the extended brainstem. The extended brainstem region of interest (1008 voxels) was computed as the conjunction of the group effect images thresholded at $z = 2.6$ for all six striatal seeds. Both groups showed a comparable striatal:extended brainstem

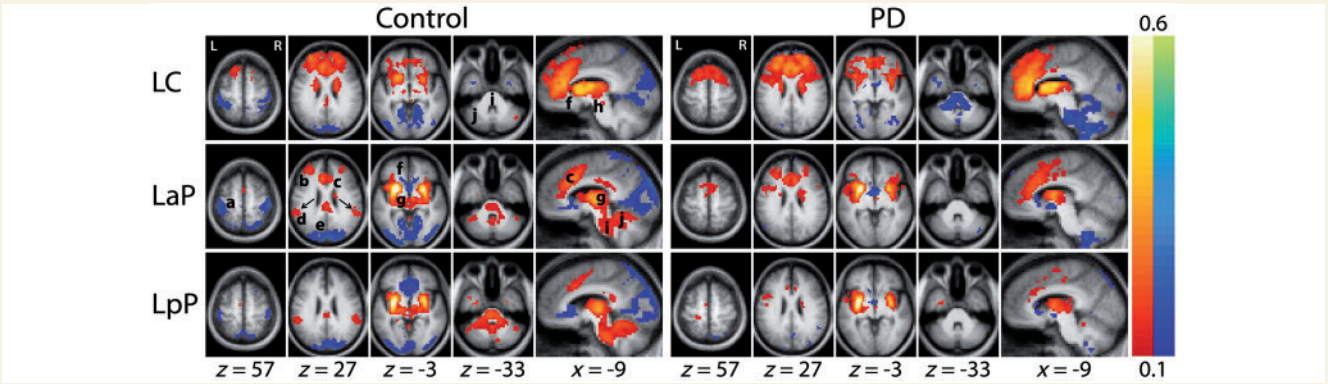

Figure 2 Striatal functional connectivity [$z(r)$ maps] averaged over subjects in the control (*left*) and Parkinson's disease groups (*right*). Each row corresponds to a distinct striatal seed region of interest. Warm and cool colours represent positive and negative correlations. The underlying image is the study-specific atlas template (see 'Materials and methods' section). The Talairach atlas plane of section is indicated under each column. The *z*, *y* and *x* correspond, respectively, to axial, coronal and sagittal sections. Similar $z(r)$ maps obtained with right hemisphere striatal seeds are shown in Supplementary Fig. 3. Arrows (control group left anterior putamen map) indicate the supramarginal gyrus bilaterally (Talairach coordinates: $\pm 55.5, -42, +27$); seeds centred on these coordinates were used to obtain the results shown Fig. 5. Letters identify local resting-state functional connectivity MRI peaks: a = sensori-motor cortex, b = fronto-polar cortex, c = anterior cingulate cortex, d = supramarginal gyrus, e = visual cortex, f = subgenual prefrontal cortex, g = thalamus, h = midbrain, i = pons and j = cerebellum. LaP = left anterior putamen; LC = left caudate; LpP = left posterior putamen; PD = Parkinson's disease.

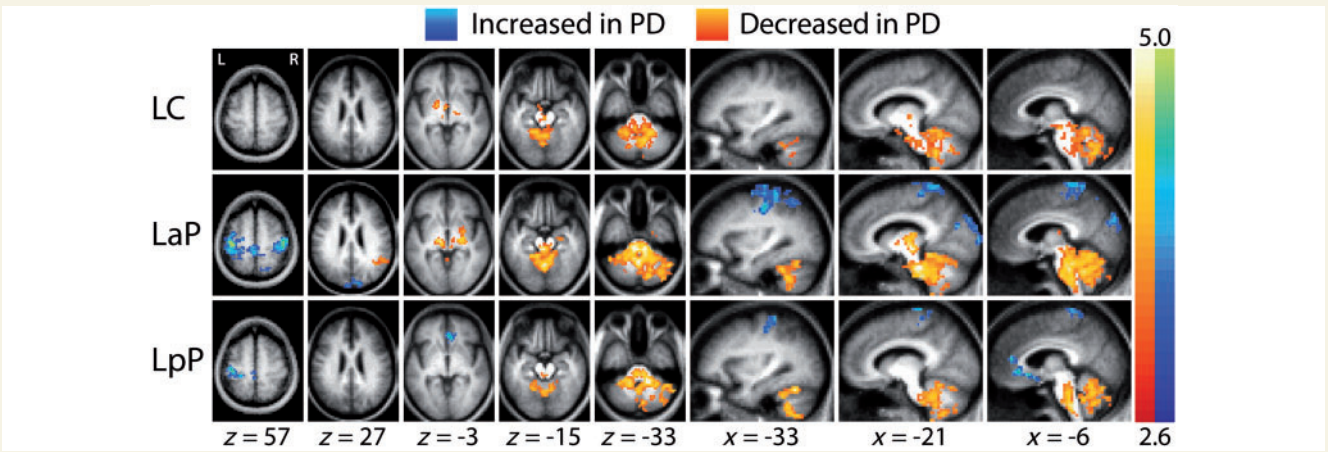

Figure 3 Random effects analysis contrasting the control versus Parkinson's disease groups. The mapped quantity is the Gaussianized *t*-statistic (*Z*-score) thresholded at $|Z| > 2.6$. All illustrated clusters are significant at the $P = 0.05$ level (Supplementary material). Left caudate, left anterior putamen and left posterior putamen as in Fig. 2. Warm colours indicate more positive correlations in the control group. Cool colours indicate more negative correlations in the control group. Similar results obtained with right hemisphere striatal seeds are shown in Supplementary Fig. 4. LaP = left anterior putamen; LC = left caudate; LpP = left posterior putamen; PD = Parkinson's disease.

functional connectivity gradient (caudate < anterior putamen < posterior putamen). However, in the Parkinson's disease group, these correlations were consistently less positive (Fig. 4A). Thus, for all six striatal seeds, the (Fisher *z*-transformed) correlation difference (control − Parkinson's disease) averaged over the extended brainstem was $\sim +0.20$. Essentially, the same findings were obtained omitting whole-brain signal regression during preprocessing, except that all correlations were shifted positively (Supplementary Fig. 5). In additional analyses, striatal:extended brainstem correlations (averaged over all six seeds) evaluated in individuals were found to be significantly correlated ($r = -0.61$, $P < 0.05$) with UPDRS III scores (Fig. 4B).

Striatal correlations with the cerebral cortex were generally shifted towards more positive values in the Parkinson's disease group. This result appears in the right half of Fig. 2 as an absence of anti-correlations in sensori-motor, visual and subgenual prefrontal regions. Statistically significant clusters corresponding to this group contrast appear in Fig. 3 (blue clusters, e.g. left anterior putamen seed, $z = 57$). We did not observe enhanced anti-correlations in the Parkinson's disease group. In a departure from the general pattern, positive putamenal correlations with the supramarginal gyrus were weaker in the Parkinson's disease group. This difference appears bilaterally in Fig. 2 (left anterior putamen seed, $z = 27$) as orange voxels and in Fig. 3 as a

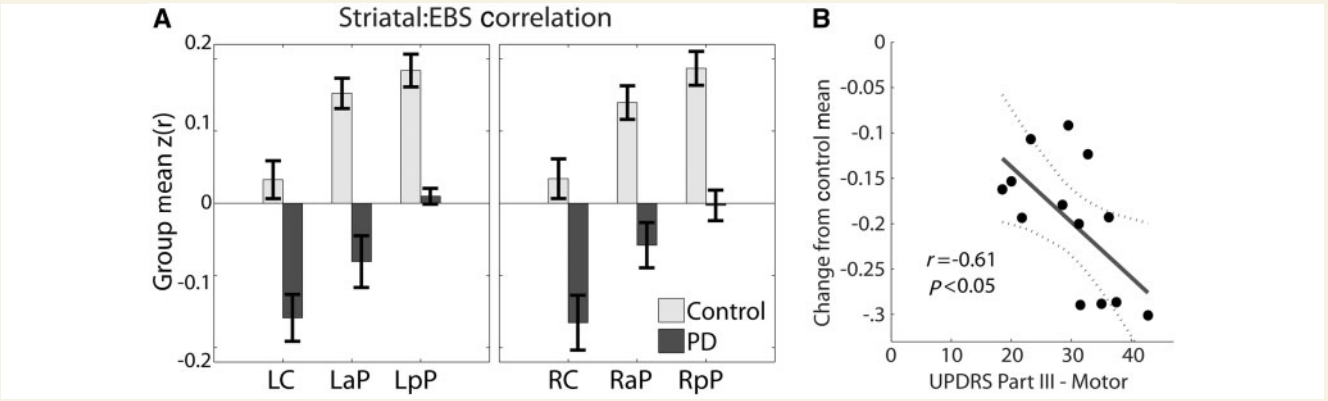

Figure 4 (**A**) Striatal functional connectivity with the extended brainstem. Fisher *z*-transformed correlations [*z*(*r*)] were evaluated in each individual by averaging over extended brainstem voxels showing a significant group effect (Fig. 3). Bar height indicates the group mean. Error bars indicate the standard error of the mean. Left caudate, left anterior putamen and left posterior putamen as in Figs 2 and 3. Right caudate, right anterior putamen and right posterior putamen indicate corresponding seed regions of interest in the right hemisphere. Note graded (caudate < anterior putamen < posterior putamen) extended brainstem correlations in both groups and systematically more negative correlations in the Parkinson's disease group. (**B**) Individual striatum:extended brainstem functional connectivity [z(*r*)] averaged over all six striatal seeds versus UPDRS III scores in each patient; *z*(*r*) values are plotted relative to the mean obtained in the control group. LaP = left anterior putamen; LC = left caudate; LpP = left posterior putamen; PD = Parkinson's disease; RaP = right anterior putamen; RC = right caudate; RpP = right posterior putamen.

significant orange cluster in the right hemisphere. supramarginal gyrus functional connectivity group differences represent a distinct effect and are described more fully later in text.

Follow-up analyses were conducted by placing seed regions of interest in cortical regions that showed group differences in correlation maps obtained with striatal seeds. The results of these analyses indicated reduced correlations between sensori-motor and visual regions in the Parkinson's disease group. These regions exhibited similar (negative) correlations with the putamen in the control group and similar effects in control versus Parkinson's disease group contrasts. As these findings corroborate the results shown in Figs 2 and 3, they are reported in Supplementary Fig. 8. However, supramarginal gyrus seeds produced results that represent a departure from the findings described earlier.

Supramarginal gyrus functional connectivity in the control group (Fig. 5A) was symmetric. In the Parkinson's disease group, it was markedly asymmetric (Fig. 5B). Thus, the maps obtained with the left supramarginal gyrus seed exhibited similar topographies in the two groups, although correlation values were relatively attenuated in the Parkinson's disease group. In contrast, the right supramarginal gyrus seed gave rise to diffusely enhanced prefrontal correlations, with statistically significant (control versus Parkinson's disease) effects involving the caudate heads bilaterally (blue clusters in Fig. 5B, $z = 15$). This diffuse prefrontal enhancement appears also in the results obtained with caudate seeds (Fig. 2 and Supplementary Fig. 3, $z = 57$, $z = 27$, $x = -9$). Asymmetry of supramarginal gyrus functional connectivity in the Parkinson's disease group also appears in Fig. 5C (orange cluster at $z = 30$) as significantly greater control versus Parkinson's disease correlations of the left supramarginal gyrus in maps obtained with the right supramarginal gyrus seed. This effect represents abnormally low inter-hemispheric supramarginal gyrus correlations.

To investigate the relation between asymmetric motor disability and asymmetric resting-state functional connectivity MRI, limb UPDRS III scores (tremor + bradykinesia + rigidity) were assessed, averaging over the ON and OFF conditions. UPDRS asymmetry then was computed as (Right − Left)/(Right + Left). A significant correlation between ipsilateral supramarginal gyrus:caudate resting-state functional connectivity MRI and UPDRS III asymmetry was found for the right ($r = 0.61$, $P < 0.03$) but not the left hemisphere (Fig. 5D). Resting-state functional connectivity MRI asymmetry was defined as the difference of the right and left hemispheres of Parkinson's disease subjects minus control effects in each hemisphere. The correlation between resting-state functional connectivity MRI asymmetry and UPDRS III asymmetry was significant ($r = 0.67$, $P < 0.012$, Fig. 5D).

The results presented so far constitute a somewhat diverse set of observations. A more unified view of Parkinson's disease versus control functional connectivity differences emerged by examination of the distributions (histograms) of correlation values compiled over the whole brain, separately for each striatal seed. Histograms representing the control group, the Parkinson's disease group and the control minus Parkinson's disease difference are shown in Fig. 6. Three territories of interest, identified by the previously described analyses, specifically, the extended brainstem, sensori-motor + visual cortex and frontal cortex, are colour-coded as partitions in the histograms. Voxels outside these territories are represented as grey. The extended brainstem subregion (yellow) was isolated from the left posterior putamen correlation map as a contiguous zone satisfying $z(r) > 0.1$. Similarly, sensori-motor + visual cortex region (green) was defined as the union of two contiguous zones satisfying $z(r) < -0.1$ in the control left anterior putamen map; the prefrontal region (orange) was defined as a contiguous zone satisfying $z(r) > 0.1$ in the Parkinson's disease left caudate map.

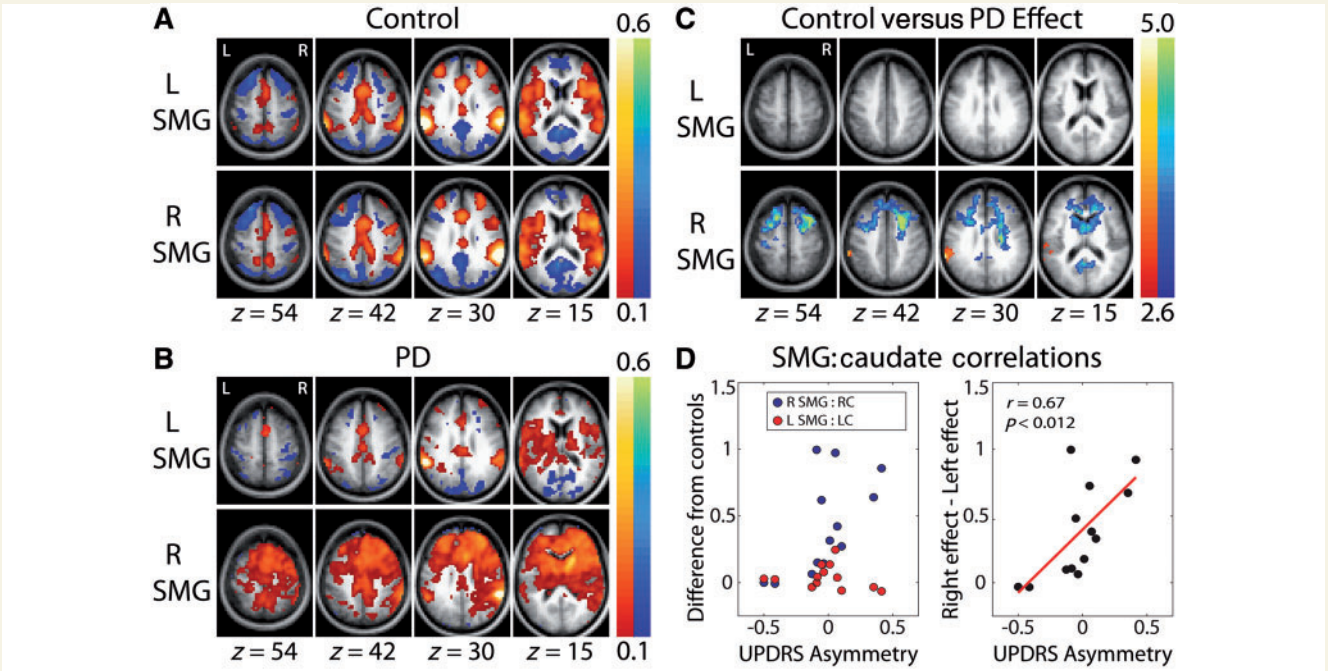

Figure 5 Group-averaged $z(r)$ maps obtained with seed regions of interest in the supramarginal gyrus (supramarginal gyrus) of each hemisphere. The seeds were defined as 7-mm radius spheres centred on the paired posterior positive foci in the control group left anterior putamen result shown in Fig. 2 ($z = 27$). (**A**) Results obtained in the control group. Positive correlations correspond to the ventral attention network. Generally, symmetric maps and comparable results were obtained with supramarginal gyrus seeds in either hemisphere. (**B**) Results obtained in the Parkinson's disease (PD) group. For the left supramarginal gyrus seed, reduced correlation magnitude in the Parkinson's disease group without major difference in topography; for the right supramarginal gyrus seed, major reorganization in the Parkinson's disease group. (**C**) Cluster-wise significant ($P < 0.05$) group contrast effects; conventions as in Fig. 3. Only the right supramarginal gyrus seed showed significant clusters in the control group versus the Parkinson's disease group. (**D**) *Left*: (patient with Parkinson's disease − control mean) supramarginal gyrus:caudate blood oxygen level-dependent correlation versus UPDRS III limb score asymmetry. Each hemisphere is plotted separately. *Right*: Right (Parkinson's disease − control mean) − Left (Parkinson's disease − control mean) supramarginal gyrus:caudate correlations versus UPDRS III limb score asymmetry.

In both groups, striatal: extended brainstem correlations (yellow partition) progressively shift leftward (negatively) as the seed moves from posterior putamen to anterior putamen to caudate; this effect reiterates the gradient of extended brainstem correlations across the striatum shown in Fig. 4A. The extended brainstem partition is consistently more negative in the Parkinson's disease group relative to the control group, which reiterates the group effect in Fig. 4A. Finally, in the control minus Parkinson's disease histograms (Fig. 6), the group difference manifests as a consistently positive yellow partition.

The histograms also demonstrate a differential impact of correlation change on striatal subdivisions. Thus, although the control minus Parkinson's disease difference histograms are nearly identical (bottom row), these differences specifically attenuate functional connectivity of the posterior putamen. That is, posterior putamen correlations with the entire brain are more tightly centred about zero in the Parkinson's disease group. This is indicated by a significant resampling test comparing the left posterior putamen histogram SD values in the Parkinson's disease and control groups. In contrast, the caudate distribution is broader in the Parkinson's disease group (Fig. 6), largely because the orange partition is relatively shifted to the right. The green partition also is relatively shifted to the right in the Parkinson's disease group. This corresponds to the presence of striatal anti-correlations in visual and sensori-motor cortices in the control group (Fig. 2) and absence of these anti-correlations in the Parkinson's disease group (Fig. 2).

Discussion

Study overview

We report a resting-state functional connectivity study comparing patients with idiopathic Parkinson's disease to age-matched control subjects. Using seed regions of interest manually defined bilaterally in three subdivisions of the striatum, the principal findings in Parkinson's disease were as follows: (i) markedly lower striatal correlations with the extended brainstem (i.e. thalamus, midbrain, upper pons and cerebellum); (ii) moderately increased striatal correlations with specific parts of the cerebral cortex; (iii) generally symmetric effects of Parkinson's disease except for correlation differences involving the supramarginal gyrus region of the cerebral cortex; and (iv) the effects of Parkinson's disease on striatal correlations were arithmetically uniform across striatal subdivisions;

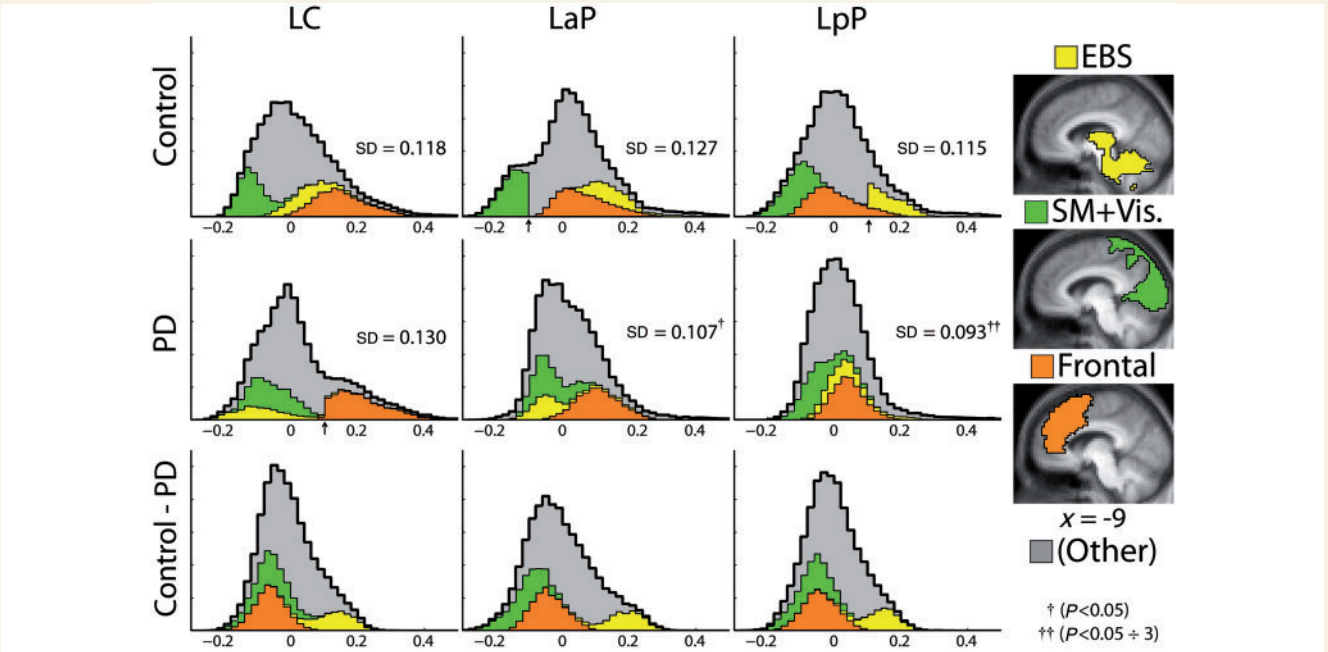

Figure 6 Correlation histograms of group-averaged *z*(*r*) values compiled over all voxels in the brain. Selected subregions of the brain, shown at the *right*, are colour-coded: yellow = extended brainstem (EBS), green = combined sensori-motor (SM) and visual (Vis) areas and orange = prefrontal region of increased caudate correlations in the Parkinson's disease group. The coloured partition of each histogram represents voxels in the corresponding subregion. The remaining voxels are grey. Abrupt partition boundaries (arrows) are a consequence of the thresholding procedure used to define the subregions. Histogram SDs (group means of SD measured in individuals) are indicated in inset text. Statistical significance of control minus Parkinson's disease histogram SD (width) was assessed by permutation resampling. The posterior putamen histogram was significantly more narrow in the Parkinson's disease group ($P < 0.05 \div 3$ comparisons). The anterior putamen histogram was narrower in the Parkinson's disease group ($P < 0.05$ uncorrected). The caudate histogram was broader (not significant); left caudate, left anterior putamen and left posterior putamen are as in Figs 2–4. The *bottom* row shows control minus Parkinson's disease difference histograms. Note the substantially similar difference histograms across striatal seed regions of interest. PD = Parkinson's disease.

however. the impact of these effects, in terms of reduced correlations of either sign with the brain as whole, was markedly different in the posterior putamen as compared with the caudate. The following discussion considers, in turn, results obtained in the control and participants with Parkinson's disease and the implications of these findings with regards to the pathophysiology of Parkinson's disease.

Results obtained in age-matched control subjects

The principal features of correlation maps obtained in the control subjects with seed regions in the striatum were as follows: (i) positive correlations with other parts of the striatum in both hemispheres, as well as the extended brainstem; (ii) positive correlations with specific frontal and parietal cortical areas associated with cognitive control (Vincent *et al*., 2008; Nelson *et al*., 2010); (iii) negative correlations with parts of sensori-motor and visual cortices; (iv) a high degree of bilateral symmetry; and (v) graded functional connectivity depending on the striatal subdivision used as seed. All of these features are evident in previously reported results obtained using similar methods (Di Martino *et al*., 2008; Kelly *et al*., 2009; Barnes *et al*., 2010). Perfect agreement cannot be expected because of variability in the selection of seed regions of interest, minor algebraic differences in mapping strategy and inconsistent coverage of the reported maps. Moreover, the subjects in prior studies were young adults, whereas the mean age here was 66 years (see Andrews-Hanna *et al*., 2007; Damoiseaux *et al*., 2008 for documentation of the considerable effects of normal ageing on resting-state functional connectivity MRI). Nevertheless, considerable similarity can be seen across studies [e.g. compare Fig. 2 in this article to Figs 1–4 in Kelly *et al*. (2009)].

Striatal functional connectivity changes in Parkinson's disease

Extended brainstem

The most prominent effect of Parkinson's disease was reduced correlations between the striatum and the entire extended brainstem (Figs 2 and 3 and Supplementary Figs 3 and 4). Moreover, this effect was approximately uniform across all striatal subdivisions (Figs 4 and 6). Parkinson's disease-related reduced functional connectivity between the striatum and the extended brainstem (or its components) has not been previously demonstrated. Loss of striatal functional connectivity with the brainstem

is concordant with the well-documented distribution of Parkinson's disease histopathology (Braak *et al*., 2004). Our findings also reinforce the relevance to parkinsonism of the recently described circuits connecting the cerebellum to the basal ganglia (Hoshi *et al*., 2005; Bostan *et al*., 2010). Also, certain clinical manifestations of Parkinson's disease, that is, sleep disturbances and dysautonomia, are increasingly attributed to brainstem dysfunction (Grinberg *et al*., 2010; Chahine and Stern, 2011). Loss of striatal:extended brainstem functional connectivity offers a plausible explanation for gait difficulties, postural instability and freezing (sudden short-lived cessation of movement), all of which suggest dysfunction of the pedunculopontine nucleus (a midbrain structure) (Pahapill and Lozano, 2000; Karimi *et al*., 2008; Snijders *et al*., 2011). Resting tremor is another major manifestation of Parkinson's disease that often is viewed as unexplained by dysfunction confined to nigrostriatal pathways. A recent functional MRI study of blood oxygen level-dependent responses linked to fluctuating arm tremor amplitude demonstrated co-activation of contralateral cerebellum, ventral intermediate thalamus and motor cortex, in addition to putamen and globus pallidus (Helmich *et al*., 2011). This set of structures substantially overlaps the extended brainstem. Similarly, the topography of Parkinson's disease-related alterations in fluorodeoxyglucose metabolism (Mure *et al*., 2011) substantially overlaps the extended brainstem.

Sensori-motor and visual cortex

Group differences in striatal correlations with the cerebral cortex were observed principally in sensori-motor and visual regions (Fig. 3 and Supplementary Fig. 4). Additional analyses (see Supplementary material) showed that these same regions also exhibited significantly reduced cortico-cortical functional connectivity (Supplementary Fig. 8). Thus, loss of striatal–cortical functional connectivity is only part of a larger picture. The topography of the affected regions plausibly corresponds to the clinical manifestations of Parkinson's disease, which is primarily a movement disorder with associated executive deficits (Carbon and Marie, 2003; Monchi *et al*., 2007) and visual disturbances (Cardoso *et al*., 2010). However, the cerebral distribution of Lewy body histopathology, even at late disease stages, does not at all correspond to the presently observed focality of cortical functional connectivity changes. In fact, according to Braak *et al*. (2004) sensori-motor and visual cortices are the last to become affected by Lewy body histopathology.

Functional connectivity changes in Parkinson's disease

Right supramarginal gyrus

Helmich *et al*. (2010) conducted a careful study similar to ours, also using seed regions in striatal subdivisions, and reported an anterior shift of putamenal (but not caudate) supramarginal gyrus functional connectivity towards more anterior subdivisions. Our results are broadly consistent with this finding, although we observed anterior shifts throughout the striatum, including the caudate. This difference in topographic emphasis most likely reflects differences in computational strategy. Helmich *et al*. (2010) based their analysis on (order 3) partial correlation, which is advantageous when the objective is to distinguish between striatal subdivisions. On the other hand, this technique is insensitive to effects that are common to all seeds, e.g. Parkinson's disease versus control differences in striatal:extended brainstem functional connectivity.

Another point of concordance concerns lateralization of supramarginal gyrus:striatal remapping. Helmich *et al*. (2010) observed that remapping was lateralized to the least affected (not necessarily the right) hemisphere. Our results suggest that supramarginal gyrus remapping occurs only in the right hemisphere but is most pronounced in patients in whom the right hemisphere is less affected (Fig. 5). Thus, both studies support the hypothesis that functional connectivity remapping reflects anterior striatal compensation for loss of function more posteriorly (Helmich *et al*., 2010). The present supramarginal gyrus resting-state functional connectivity MRI group differences were asymmetrically right-sided, whereas all other findings were symmetrical. Right-lateralized topography, similar to the right supramarginal gyrus correlation map in the Parkinson's disease group (Fig. 5B), has been reported in motor task functional MRI responses in asymptomatic carriers of the mutant parkin allele (Buhmann *et al*., 2005). These effects may be related to compromised functional connectivity of a particular resting-state network: the anterior cingulate cortex, anterior insula, dorsolateral prefrontal cortex and right supramarginal gyrus together constitute the ventral attention network (Yeo *et al*., 2011). This network, which is asymmetrically represented in the right hemisphere (Fox *et al*., 2006), is recruited by orienting to unexpected stimuli (Corbetta and Shulman, 2002). In our data, the ventral attention network is topographically well defined in the control group (Fig. 5A) but not the Parkinson's disease group (Fig. 5B). This difference may underlie the characteristic impairment of attentional mechanisms in Parkinson's disease (Leh *et al*., 2010).

Levodopa

Unmedicated patients with Parkinson's disease are prone to tremor or dystonia. This is an important point because, as recently demonstrated, motion-related artefacts are especially problematic in resting-state functional MRI studies (Power *et al*., 2012; Satterthwaite *et al*., 2012; Van Dijk *et al*., 2012). Apart from artefact, adventitious movements generate sensory feedback, which potentially confounds the interpretation of neuroimaging findings (Hershey and Mink, 2006). For all of these reasons, our experimental paradigm does not involve imaging patients with Parkinson's disease OFF L-DOPA medication.

L-DOPA administration in normal young adults induces functional connectivity changes opposite to the presently observed Parkinson's disease versus control differences (Kelly *et al*., 2009). The topographies of these effects [Figs 1–4 in Kelly *et al*. (2009)] bear remarkable similarity to our control versus Parkinson's disease differences (Fig. 2 and Supplementary Fig. 3). It is parsimonious to assume that L-DOPA acts similarly in healthy controls and patients with Parkinson's disease. Here, it is critical to note that our Parkinson's disease group exhibited functional connectivity changes opposite to those described by Kelly *et al*. (2009), despite

treatment with L-DOPA. Thus, it appears that L-DOPA does not fully reverse the resting-state functional connectivity MRI changes attributable to Parkinson's disease. Several functional MRI studies (resting state and task-based) have reported that L-DOPA 'normalizes' results in patients with Parkinson's disease, that is, causes features in the data to more closely resemble those observed in control subjects (Wu *et al*., 2009; Palmer *et al*., 2010; Rowe *et al*., 2010). Such results imply that the presently observed Parkinson's disease versus control differences would have been even more pronounced had our patients been studied OFF medication (disregarding the earlier discussed technical complications associated with subject motion).

Relation to positron emission tomography studies of dopaminergic function

PET studies of dopaminergic function (Kuriakose and Stoessl, 2010; Brooks and Pavese, 2011; Gallagher *et al*., 2011), as well as post-mortem histochemistry studies (Kish *et al*., 1988; Wilson *et al*., 1996; Goldstein *et al*., 2011), indicate that striatal dopaminergic function is lost in a graded distribution (posterior putamen > anterior putamen > caudate). Here, the posterior putamen, in patients with Parkinson's disease compared with control subjects, showed weaker correlations of either sign with the brain as a whole, whereas the caudate was spared by this measure (Fig. 6). In other words, the posterior putamen in Parkinson's disease appears to lose functional connectivity with the rest of brain. This posterior putamen versus caudate distinction follows the same gradient as dopamine function loss in Parkinson's disease. The pathophysiological link between these phenomena, if any, is completely unknown. The same gradient (posterior putamen > anterior putamen > caudate) was present (and to the same extent) in the striatal:extended brainstem correlations obtained in both groups (Fig. 4). Thus, the group differences in striatal:extended brainstem correlations were similar across striatal subdivisions. In fact, the control minus Parkinson's disease group differences in the distributions of striatal correlations with the brain as a whole were remarkably similar across striatal subdivisions (Fig. 6).

The results shown in Fig. 6 may appear to show contradictory results. However, there is no contradiction: increased positive correlations together with decreased negative correlations generate the same distribution of changes as increased negative correlations together with decreased positive correlations. The posterior putamen is normally more functionally connected with the extended brainstem, and the caudate is normally more functionally connected with the cerebral cortex. In Parkinson's disease, striatal correlations with the extended brainstem (positive) are reduced, whereas striatal correlations with the cerebral cortex (negative) are increased. Thus, posterior putamen correlations of either sign tend towards zero, whereas the functional connectivity of the caudate is unaffected or even enhanced. A schematized version of the underlying principle is illustrated in Fig. 7.

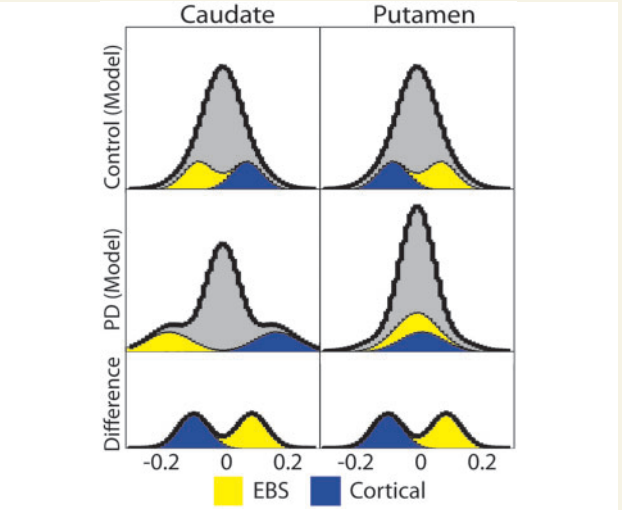

Figure 7 Schematized version of Fig. 6. Extended brainstem (EBS, yellow), cortex subregion (blue) and remaining (grey) voxels are modelled as Gaussian distributions. *Top* (control group): putamen:extended brainstem correlations are more positive than putamen:cortex correlations; caudate:extended brainstem correlations are less positive than caudate:cortex correlations. *Middle* (Parkinson's disease group): striatal:extended brainstem and striatal:cortex correlation are identically shifted in both caudate and putamen relative to the control group. This shift causes putamen:extended brainstem and putamen:cortex correlations to be centred on zero, narrowing the putamen histrogram, whereas the caudate distribution becomes broader. *Bottom*: histogram of control minus Parkinson's disease differences is the same for caudate and putamen. PD = Parkinson's disease.

A hypothesis concerning pathogenesis

The striatum and the brainstem currently are thought to be two of the most important brain structures in the pathophysiology of Parkinson's disease. Our results also show a gradient of striatal:extended brainstem correlations (posterior putamen > anterior putamen > caudate) in the control and the Parkinson's disease groups. We speculate that this gradient underlies the differential susceptibility to cellular dysfunction in Parkinson's disease, specifically dopaminergic function loss as imaged by PET. This suggestion is in line with the recently articulated hypothesis that functional connectivity in health predicts differential susceptibility to pathology in neurodegenerative diseases (Zhou *et al*., 2012). Thus, identifying the lower brainstem as the epicentre of disease in Parkinson's disease, differential involvement of the posterior putamen may be a consequence of its greater functional connectivity with the brainstem. It has been shown that synaptic dysfunction can be induced via axonal connections to pathological tissue even without transfer of toxic molecular species (Harris *et al*., 2010). Direct axonal connections are not known to exist between the lower brainstem and posterior putamen (Winn *et al*., 2010), but such connections are not required by the Zhou *et al*. (2012) hypothesis. Thus, the correspondence between the striatal:extended brainstem gradient of blood oxygen level-depndent correlations in

health, as well as disease, and the characteristic PET findings in Parkinson's disease may not be a coincidence.

Study limitations

The present study is limited principally by the relatively small size of the subject samples. However, this limitation is, in part, a consequence of the rigorous quality assurance standards applied to the acquired functional MRI data, which we regard as a study strength. Our results need to be replicated. Much larger sample sizes may permit identification of resting-state effects specific to tremor-dominant versus rigidity dominant subpopulations (Lewis *et al*., 2011). There exists the formal possibility that our group contrasts reflect medication effects rather than Parkinson's disease. However, this interpretation requires the assumption that the effects of L-DOPA reverse the sign in young versus older individuals with Parkinson's disease. This is unlikely [in fact, contradicted by limited evidence; Hershey *et al*., (2003)]. Not including a comparison of the medicated versus unmedicated state may be counted as a formal limitation. However, resting-state studies of unmedicated patients are challenging. It is potentially feasible to reduce motion-related artefacts using regression techniques (Helmich *et al*., 2010), but the effectiveness of this strategy is uncertain (Power *et al*., 2012).

Acknowledgements

The authors thank Johanna Hartlein for assistance with the Parkinson's disease patients. They also thank Dr John Morris and the Washington University Alzheimer's Disease Research Group for making available age-matched control subjects. In addition, they thank Tim Laumann for helpful discussion and analysis suggestions.

Funding

This work was supported by the following: National Institute of Mental Health (K23MH081786 to B.A.), National Institute of Nursing Research (R01NR012907, R01NR012657 to B.A.), National Institute of Health (NS41509, NS075321, NS058714, RR024992 to J.P. and P50NS006833 to A.S.), National Institute of Neurologic Disorders and Stroke (P30 NS048056 to A.S.) and American Parkinson Disease Association (APDA); Greater St. Louis Chapter of the APDA, Barnes Jewish Hospital Foundation (Elliot Stein Endowment and Parkinson Disease research fund) and McDonnell Center for Higher Brain Function (to J.P.).

Supplementary material

Supplementary material is available at *Brain* online.

References

Albin RL, Young AB, Penney JB. The functional anatomy of basal ganglia disorders. Trends Neurosci 1989; 12: 366–75.

Alexander GE, DeLong MR, Strick PL. Parallel organization of functionally segregated circuits linking basal ganglia and cortex. Annu Rev Neurosci 1986; 9: 357–81.

Andrews-Hanna JR, Snyder AZ, Vincent JL, Lustig C, Head D, Raichle ME, et al. Disruption of large-scale brain systems in advanced aging. Neuron 2007; 56: 924–35.

Barnes KA, Cohen AL, Power JD, Nelson sensori-motor, Dosenbach YB, Miezin FM, et al. Identifying Basal Ganglia divisions in individuals using resting-state functional connectivity MRI. Front Syst Neurosci 2010; 4: 18.

Berardelli A, Rothwell JC, Thompson PD, Hallett M. Pathophysiology of bradykinesia in Parkinson's disease. Brain 2001; 124 (Pt 11): 2131–46.

Biswal B, Yetkin FZ, Haughton VM, Hyde JS. Functional connectivity in the motor cortex of resting human brain using echo-planar MRI. Magn Reson Med 1995; 34: 537–41.

Bostan AC, Dum RP, Strick PL. The basal ganglia communicate with the cerebellum. Proc Natl Acad Sci USA 2010; 107: 8452–6.

Braak H, Ghebremedhin E, Rub U, Bratzke H, Del Tredici K. Stages in the development of Parkinson's disease-related pathology. Cell Tissue Res 2004; 318: 121–34.

Brooks DJ, Pavese N. Imaging biomarkers in Parkinson's disease. Prog Neurobiol 2011; 95: 614–28.

Buckner RL, Andrews-Hanna JR, Schacter DL. The brain's default network: anatomy, function, and relevance to disease. Ann N Y Acad Sci 2008; 1124: 1–38.

Buckner RL, Head D, Parker J, Fotenos AF, Marcus D, Morris JC, et al. A unified approach for morphometric and functional data analysis in young, old, and demented adults using automated atlas-based head size normalization: reliability and validation against manual measurement of total intracranial volume. Neuroimage 2004; 23: 724–38.

Buckner RL, Krienen FM, Castellanos A, Diaz JC, Yeo BT. The organization of the human cerebellum estimated by intrinsic functional connectivity. J Neurophysiol 2011; 106: 2322–45.

Buckner RL, Snyder AZ, Shannon BJ, LaRossa G, Sachs R, Fotenos AF, et al. Molecular, structural, and functional characterization of Alzheimer's disease: evidence for a relationship between default activity, amyloid, and memory. J Neurosci 2005; 25: 7709–17.

Buhmann C, Binkofski F, Klein C, Buchel C, van Eimeren T, Erdmann C, et al. Motor reorganization in asymptomatic carriers of a single mutant Parkin allele: a human model for presymptomatic parkinsonism. Brain 2005; 128 (Pt 10): 2281–90.

Carbon M, Marie RM. Functional imaging of cognition in Parkinson's disease. Curr Opin Neurol 2003; 16: 475–80.

Cardoso EF, Fregni F, Maia FM, Melo LM, Sato JR, Cruz AC Jr, et al. Abnormal visual activation in Parkinson's disease patients. Mov Disord 2010; 25: 1590–6.

Catalan MJ, Ishii K, Honda M, Samii A, Hallett M. A PET study of sequential finger movements of varying length in patients with Parkinson's disease. Brain 1999; 122 (Pt 3): 483–95.

Chahine LM, Stern MB. Diagnostic markers for Parkinson's disease. Curr Opin Neurol 2011; 24: 309–17.

Corbetta M, Shulman GL. Control of goal-directed and stimulus-driven attention in the brain. Nat Rev Neurosci 2002; 3: 201–15.

Damier P, Hirsch EC, Agid Y, Graybiel AM. The substantia nigra of the human brain: part II. Patterns of loss of dopamine-containing neurons in Parkinson's disease. Brain 1999; 122 (Pt 8): 1437–48.

Damoiseaux JS, Beckmann CF, Arigita EJ, Barkhof F, Scheltens P, Stam CJ, et al. Reduced resting-state brain activity in the "default network" in normal aging. Cereb Cortex 2008; 18: 1856–64.

Del Tredici K, Rub U, De Vos RA, Bohl JR, Braak H. Where does parkinson disease pathology begin in the brain? J Neuropathol Exp Neurol 2002; 61: 413–26.

Di Martino A, Scheres A, Margulies DS, Kelly AM, Uddin LQ, Shehzad Z, et al. Functional connectivity of human striatum: a resting state FMRI study. Cereb Cortex 2008; 18: 2735–47.

Eidelberg D. Metabolic brain networks in neurodegenerative disorders: a functional imaging approach. Trends Neurosci 2009; 32: 548–57.

Fox MD, Corbetta M, Snyder AZ, Vincent JL, Raichle ME. Spontaneous neuronal activity distinguishes human dorsal and ventral attention systems. Proc Natl Acad Sci USA 2006; 103: 10046–51.

Fox MD, Greicius M. Clinical applications of resting state functional connectivity. Front Syst Neurosci 2010; 4: 19.

Fox MD, Snyder AZ, Vincent JL, Corbetta M, Van Essen DC, Raichle ME. The human brain is intrinsically organized into dynamic, anticorrelated functional networks. Proc Natl Acad Sci USA 2005; 102: 9673–8.

Fox MD, Zhang D, Snyder AZ, Raichle ME. The global signal and observed anticorrelated resting state brain networks. J Neurophysiol 2009; 101: 3270–83.

Gallagher CL, Oakes TR, Johnson SC, Chung MK, Holden JE, Bendlin BB, et al. Rate of 6-[18F]fluorodopa uptake decline in striatal subregions in Parkinson's disease. Mov Disord 2011; 26: 614–20.

Goldstein DS, Sullivan P, Holmes C, Kopin IJ, Basile MJ, Mash DC. Catechols in post-mortem brain of patients with Parkinson disease. Eur J Neurol 2011; 18: 703–10.

Grafton ST. Contributions of functional imaging to understanding parkinsonian symptoms. Curr Opin Neurobiol 2004; 14: 715–19.

Grinberg LT, Rueb U, Alho AT, Heinsen H. Brainstem pathology and non-motor symptoms in PD. J Neurol Sci 2010; 289: 81–8.

Harris JA, Devidze N, Verret L, Ho K, Halabisky B, Thwin MT, et al. Transsynaptic progression of amyloid-beta-induced neuronal dysfunction within the entorhinal-hippocampal network. Neuron 2010; 68: 428–41.

Helmich RC, Derikx LC, Bakker M, Scheeringa R, Bloem BR, Toni I. Spatial remapping of cortico-striatal connectivity in Parkinson's disease. Cereb Cortex 2010; 20: 1175–86.

Helmich RC, Janssen MJ, Oyen WJ, Bloem BR, Toni I. Pallidal dysfunction drives a cerebellothalamic circuit into Parkinson tremor. Ann Neurol 2011; 69: 269–81.

Hershey T, Mink JW. Using functional neuroimaging to study the brain's response to deep brain stimulation. Neurology 2006; 66: 1142–3.

Hershey T, Revilla FJ, Wernle AR, McGee-Minnich L, Antenor JV, Videen TO, et al. Cortical and subcortical blood flow effects of subthalamic nucleus stimulation in PD. Neurology 2003; 61: 816–21.

Hoshi E, Tremblay L, Feger J, Carras PL, Strick PL. The cerebellum communicates with the basal ganglia. Nat Neurosci 2005; 8: 1491–3.

Hughes AJ, Daniel SE, Kilford L, Lees AJ. Accuracy of clinical diagnosis of idiopathic Parkinson's disease: a clinico-pathological study of 100 cases. J Neurol Neurosurg Psychiatry 1992; 55: 181–4.

Jankovic J. Parkinson's disease: clinical features and diagnosis. J Neurol Neurosurg Psychiatry 2008; 79: 368–76.

Karimi M, Golchin N, Tabbal SD, Hershey T, Videen TO, Wu J, et al. Subthalamic nucleus stimulation-induced regional blood flow responses correlate with improvement of motor signs in Parkinson disease. Brain 2008; 131 (Pt 10): 2710–19.

Kelly C, de Zubicaray G, Di Martino A, Copland DA, Reiss PT, Klein DF, et al. L-dopa modulates functional connectivity in striatal cognitive and motor networks: a double-blind placebo-controlled study. J Neurosci 2009; 29: 7364–78.

Kish SJ, Shannak K, Hornykiewicz O. Uneven pattern of dopamine loss in the striatum of patients with idiopathic Parkinson's disease. Pathophysiologic and clinical implications. N Engl J Med 1988; 318: 876–80.

Kuriakose R, Stoessl AJ. Imaging the nigrostriatal system to monitor disease progression and treatment-induced complications. Prog Brain Res 2010; 184: 177–92.

Kwak Y, Peltier S, Bohnen NI, Muller ML, Dayalu P, Seidler RD. Altered resting state cortico-striatal connectivity in mild to moderate stage Parkinson's disease. Front Syst Neurosci 2010; 4: 143.

Lancaster JL, Glass TG, Lankipalli BR, Downs H, Mayberg H, Fox PT. A modality-independent approach to spatial normalization of tomographic images of the human brain. Hum Brain Mapp 1995; 3: 209–23.

Leh SE, Petrides M, Strafella AP. The neural circuitry of executive functions in healthy subjects and Parkinson's disease. Neuropsychopharmacology 2010; 35: 70–85.

Lewis MM, Du G, Sen S, Kawaguchi A, Truong Y, Lee S, et al. Differential involvement of striato- and cerebello-thalamo-cortical pathways in tremor- and akinetic/rigid-predominant Parkinson's disease. Neuroscience 2011; 177: 230–9.

Mevel K, Chetelat G, Eustache F, Desgranges B. The default mode network in healthy aging and Alzheimer's disease. Int J Alzheimers Dis 2011; 2011: 535816.

Mink JW. The Basal Ganglia and involuntary movements: impaired inhibition of competing motor patterns. Arch Neurol 2003; 60: 1365–8.

Monchi O, Petrides M, Mejia-Constain B, Strafella AP. Cortical activity in Parkinson's disease during executive processing depends on striatal involvement. Brain 2007; 130 (Pt 1): 233–44.

Mure H, Hirano S, Tang CC, Isaias IU, Antonini A, Ma Y, et al. Parkinson's disease tremor-related metabolic network: characterization, progression, and treatment effects. Neuroimage 2011; 54: 1244–53.

Nandhagopal R, McKeown MJ, Stoessl AJ. Functional imaging in Parkinson disease. Neurology 2008; 70 (16 Pt 2): 1478–88.

Nelson PT, Braak H, Markesbery WR. Neuropathology and cognitive impairment in Alzheimer disease: a complex but coherent relationship. J Neuropathol Exp Neurol 2009; 68: 1–14.

Nelson sensori-motor, Cohen AL, Power JD, Wig GS, Miezin FM, Wheeler ME, et al. A parcellation scheme for human left lateral parietal cortex. Neuron 2010; 67: 156–70.

Ojemann JG, Buckner RL, Corbetta M, Raichle ME. Imaging studies of memory and attention. Neurosurg Clin N Am 1997; 8: 307–19.

Pahapill PA, Lozano AM. The pedunculopontine nucleus and Parkinson's disease. Brain 2000; 123 (Pt 9): 1767–83.

Palmer SJ, Li J, Wang ZJ, McKeown MJ. Joint amplitude and connectivity compensatory mechanisms in Parkinson's disease. Neuroscience 2010; 166: 1110–18.

Power JD, Barnes KA, Snyder AZ, Schlaggar BL, Petersen SE. Spurious but systematic correlations in functional connectivity MRI networks arise from subject motion. Neuroimage 2012; 59: 2142–54.

Prodoehl J, Spraker M, Corcos D, Comella C, Vaillancourt D. Blood oxygenation level-dependent activation in basal ganglia nuclei relates to specific symptoms in de novo Parkinson's disease. Mov Disord 2010; 25: 2035–43.

Ramnani N. The primate cortico-cerebellar system: anatomy and function. Nat Rev Neurosci 2006; 7: 511–22.

Rolheiser TM, Fulton HG, Good KP, Fisk JD, McKelvey JR, Scherfler C, et al. Diffusion tensor imaging and olfactory identification testing in early-stage Parkinson's disease. J Neurol 2011; 258: 1254–60.

Rowe JB, Hughes LE, Barker RA, Owen AM. Dynamic causal modelling of effective connectivity from fMRI: are results reproducible and sensitive to Parkinson's disease and its treatment? Neuroimage 2010; 52: 1015–26.

Satterthwaite TD, Wolf DH, Loughead J, Ruparel K, Elliott MA, Hakonarson H, et al. Impact of in-scanner head motion on multiple measures of functional connectivity: Relevance for studies of neurodevelopment in youth. Neuroimage 2012; 60: 623–32.

Shin J, Kepe V, Small GW, Phelps ME, Barrio JR. Multimodal imaging of alzheimer pathophysiology in the brain's default mode network. Int J Alzheimers Dis 2011; 2011: 687945.

Shulman GL, Pope DL, Astafiev SV, McAvoy MP, Snyder AZ, Corbetta M. Right hemisphere dominance during spatial selective attention and target detection occurs outside the dorsal frontoparietal network. J Neurosci 2010; 30: 3640–51.

Skidmore F, Korenkevych D, Liu Y, He G, Bullmore E, Pardalos PM. Connectivity brain networks based on wavelet correlation analysis in Parkinson fMRI data. Neurosci Lett 2011; 499: 47–51.

Snijders AH, Leunissen I, Bakker M, Overeem S, Helmich RC, Bloem BR, et al. Gait-related cerebral alterations in patients with Parkinson's disease with freezing of gait. Brain 2011; 134 (Pt 1): 59–72.

Stoessl AJ. Functional imaging studies of non-motoric manifestations of Parkinson's disease. Parkinsonism Relat Disord 2009; 15 (Suppl 3): S13–16.

Stoessl AJ. Neuroimaging in Parkinson's disease. Neurotherapeutics 2011; 8: 72–81.

Teng EL, Chui HC. The Modified Mini-Mental State (3MS) examination. J Clin Psychiatry 1987; 48: 314–18.

Turner RS, Grafton ST, McIntosh AR, DeLong MR, Hoffman JM. The functional anatomy of parkinsonian bradykinesia. Neuroimage 2003; 19: 163–79.

Van Dijk KR, Sabuncu MR, Buckner RL. The influence of head motion on intrinsic functional connectivity MRI. Neuroimage 2012; 59: 431–8.

van Eimeren T, Monchi O, Ballanger B, Strafella AP. Dysfunction of the default mode network in Parkinson disease: a functional magnetic resonance imaging study. Arch Neurol 2009; 66: 877–83.

Vincent JL, Kahn I, Snyder AZ, Raichle ME, Buckner RL. Evidence for a frontoparietal control system revealed by intrinsic functional connectivity. J Neurophysiol 2008; 100: 3328–42.

Vincent JL, Snyder AZ, Fox MD, Shannon BJ, Andrews JR, Raichle ME, et al. Coherent spontaneous activity identifies a hippocampal-parietal memory network. J Neurophysiol 2006; 96: 3517–31.

Wilson JM, Levey AI, Rajput A, Ang L, Guttman M, Shannak K, et al. Differential changes in neurochemical markers of striatal dopamine nerve terminals in idiopathic Parkinson's disease. Neurology 1996; 47: 718–26.

Winn P, Wilson DI, Redgrave P. Subcortical connections of the basal ganglia. In: Handbook of Basal Ganglia Structure and Function. In: Steiner H, Tseng K-Y, editors. Elsevier. London, UK: Academic Press; 2010. p. 397–408.

Wu T, Hallett M. A functional MRI study of automatic movements in patients with Parkinson's disease. Brain 2005; 128 (Pt 10): 2250–9.

Wu T, Wang L, Chen Y, Zhao C, Li K, Chan P. Changes of functional connectivity of the motor network in the resting state in Parkinson's disease. Neurosci Lett 2009; 460: 6–10.

Yeo BT, Krienen FM, Sepulcre J, Sabuncu MR, Lashkari D, Hollinshead M, et al. The organization of the human cerebral cortex estimated by intrinsic functional connectivity. J Neurophysiol 2011; 106: 1125–65.

Yu H, Sternad D, Corcos DM, Vaillancourt DE. Role of hyperactive cerebellum and motor cortex in Parkinson's disease. Neuroimage 2007; 35: 222–33.

Zhang D, Raichle ME. Disease and the brain's dark energy. Nat Rev Neurol 2010; 6: 15–28.

Zhou J, Gennatas ED, Kramer JH, Miller BL, Seeley WW. Predicting regional neurodegeneration from the healthy brain functional connectome. Neuron 2012; 73: 1216–27.